

Article ID: 1001-3555(2020)01-0036-09

## CeO<sub>2</sub> Supported NiCo Bimetal Catalyzes Liquid Phase Hydrogenation of Phenol

LU Jin-zhi<sup>1,2</sup>, MA Zhan-wei<sup>1</sup>, WEI Xue-mei<sup>1,2</sup>, ZHANG Qin-sheng<sup>1</sup>, HU Bin<sup>1\*</sup>

(1. State Key Laboratory for Oxo Synthesis and Selective Oxidation, Lanzhou Institute of Chemical Physics, Chinese Academy of Sciences, Lanzhou 730000, China;

2. University of Chinese Academy of Sciences, Beijing 100049, China)

**Abstract:** CeO<sub>2</sub> nanorods-supported CoNi bimetallic catalysts was prepared by a simple wet chemical impregnation method, and the catalytic activity was tested by the hydrogenation of phenol to cyclohexanol at 150 °C under 3 MPa H<sub>2</sub>. It was found that Ni-Co/*r*-CeO<sub>2</sub> (Ni : Co = 1 : 1) catalysts showed higher activity than monometallic catalysts. The formation and dispersion of the NiCo alloy is demonstrated by Transmission electron microscopy (TEM) and X-ray powder diffraction (XRD). Temperature programmed reduction of H<sub>2</sub> (H<sub>2</sub>-TPR) and temperature programmed desorption of CO<sub>2</sub> (CO<sub>2</sub>-TPD) revealed the electronic interaction between the cobalt and nickel in the alloy, which causes the interaction force between the metal and the carrier to change. The formation of NiCo alloy changes the electronic states of Ni and Co was also revealed by X-ray photoelectron spectroscopy (XPS). Combined with the characterization results and phenol conversion, it is shown that the addition of Co modulates the surface properties of the active sites, which in turn affects the catalytic activity of metallic NiCo in the phenol hydrogenation reaction.

**Key words:** cobalt; nickel; bimetal; phenol hydrogenation; electronic effect

**CLC number:** O643.36      **Document code:** A

Cyclohexanol is an important intermediate for the production of nylon 6 and nylon 66 commodities, and an important raw material for petrochemicals and fine chemicals. Hydrogenation of phenol to cyclohexanol is widely used in industrial production due to its low energy consumption, good atomic economy, and good selectivity<sup>[1-3]</sup>. The non-precious metal Ni catalyst is widely used in the hydrogenation reaction of functional groups such as benzene ring, —C = O, —C = N and C ≡ C bond due to its good catalytic hydrogenation performance, and plays a significant role in industrial production<sup>[4-7]</sup>. While Ni catalysts have gained wide spread use in industry, they suffer from inferior mechanical strength, poor reusability and complicated post-treatment procedure<sup>[8]</sup>. Researchers have realized that single-component Ni catalysts are difficult to meet

the technological advances in terms of catalyst activity, selectivity and stability<sup>[9]</sup>. Accordingly, the design and synthesis of functional bimetallic alloys are of great interest because their structures and properties can be tuned by adjusting the elemental clusters, and bimetallic catalysts always tend to exhibit better performance than single metal catalysts<sup>[10-11]</sup>. Among all the bimetallic catalysts, platinum-group metals are the most studied components, but the high cost limits their large-scale application in industry. Ni has an electronic property similar to that of the platinum-group metals, and can be alloyed with many non-precious metals in different proportions to prepare a series of Ni-based bimetallic catalysts with different compositions, such as NiFe<sup>[12]</sup>, NiCu<sup>[13-14]</sup>, NiMg<sup>[15]</sup>, NiAl<sup>[16]</sup>, etc. They can provide more regulatory parameters to optimize

**Received date:** 2019-11-10; **Revised date:** 2019-12-10.

**Foundation:** This research was financially supported by the CAS "Light of West China" Program.

**First author:** LU Jin-zhi, female, born in 1994, master.

**Corresponding author:** E-mail: hcom@licp.cas.cn; Tel.: +86 931 4968258; fax: +86 931 8277088.

their electronic and chemical properties for high activity, selectivity and stability.

NiCo, one of the most widely studied bimetallic catalysts, has attracted much attention in the field of heterogeneous catalysis. For instance, Victor, *et al.*<sup>[17]</sup>. Investigated the catalytic performance of NiCo/ZrO<sub>2</sub> catalysts in the dry reforming reaction of methane. They found that the monometallic cobalt catalyst is inactive and the NiCo bimetallic catalysts have much better activity and selectivity in the dry reforming reaction of methane, which attributed to the adjacent Ni and Co sites hinder the deactivation of the Co single sites and the partial oxidation of the both metal under reaction conditions. Katsuya, *et al.*<sup>[18]</sup> prepared high performance CoNi/Al<sub>2</sub>O<sub>3</sub> catalysts by an impregnation method for Fischer-Tropsch synthesis to study the effect of the impregnation sequences, indicating that catalysts with Co-rich surface would be superior to those with Ni-rich surface. NiCo catalysts also attracted great interest in hydrogenation reactions. Xie and his colleague<sup>[19]</sup> reported flower-like NiCo/C bimetallic catalysts for the selective hydrogenation of *o*-chloronitrobenzene, revealing that the high performance of NiCo/C catalysts were due to a synergistic interaction between the Co and Ni species. Shi *et al.*<sup>[20]</sup> prepared NiCo/ $\gamma$ -Al<sub>2</sub>O<sub>3</sub> catalysts for the hydrogenation of phenol to cyclohexanol. Furthermore, CeO<sub>2</sub> has been widely used as an excellent supporting oxide due to the reversible Ce<sup>4+</sup>/Ce<sup>3+</sup> redox pair, rich oxygen vacancies and resulting in the electronic metal-support interactions with metal particle<sup>[21-23]</sup>. However, to date, there seems to be no research on the NiCo bimetallic catalysts with CeO<sub>2</sub> as support for the hydrogenation of phenol.

In this work, we have prepared a series of NiCo bimetallic catalysts supported on CeO<sub>2</sub> nanorods (*r*-CeO<sub>2</sub>) for the liquid-phase hydrogenation of phenol. The catalysts were characterized by TEM, XRD, TPR, TPD, and XPS techniques to evaluate the structure changes of adding Co to Ni immobilized on the *r*-CeO<sub>2</sub>. The structure-activity relationship between NiCo bimetallic catalysts and the hydrogenation of phenol was also investigated.

## 1 Experimental

### 1.1 Chemicals

All samples were purchased from Macklin Industrial Corporation in China, and were used without further purification. The purity of all gases used in the experiment was 99.999%. The deionized water resistivity in all reactions was 18.25 mol/L $\Omega$  cm.

### 1.2 Synthesis of CeO<sub>2</sub> nanorod

CeO<sub>2</sub> nanorod (*r*-CeO<sub>2</sub>) support was prepared via an improved hydrothermal method, as previously reported<sup>[24]</sup>. Firstly, 6.96 g of Ce(NO<sub>3</sub>)<sub>3</sub> · 6H<sub>2</sub>O and 19.6 g of NaOH were dissolved in 5 and 35 mL of deionized water, respectively. Subsequently, these two solutions were mixed and directly transferred to a 50 mL teflonlined stainless steel autoclave without stirring, and then heated at 100 °C for 24 h to obtain *r*-CeO<sub>2</sub>. After the hydrothermal treatment, the precipitates were washed with deionized water until the pH = 7, and then dried at 60 °C for 12 h, followed by calcination at 450 °C for 4 h in air at a heating rate of 2.5 °C/min.

### 1.3 Preparation of catalysts

NiCo/*r*-CeO<sub>2</sub> catalysts were prepared by wetness impregnation method and the total loadings were 30% (Percent weight). Firstly, the CeO<sub>2</sub> nanorod support was stirred with a solution of nickel nitrate in deionized water at room temperature for 12 h and vacuum dried overnight. Then the sample was stirred with a solution of cobalt carbonyl in hexane at room temperature for 12 h, the mixture also was vacuum dried overnight and reduced in H<sub>2</sub> flow at 450 °C for 2 h. For comparison, Ni/*r*-CeO<sub>2</sub> and Co/*r*-CeO<sub>2</sub> were prepared using the same procedures. In order to facilitate the distinction, the catalysts with different Ni and Co loadings were named as 30Co/*r*-CeO<sub>2</sub>, 5Ni-25Co/*r*-CeO<sub>2</sub>, 10Ni-20Co/*r*-CeO<sub>2</sub>, 15Ni-15Co/*r*-CeO<sub>2</sub>, 20Ni-10Co/*r*-CeO<sub>2</sub>, 25Ni-5Co/*r*-CeO<sub>2</sub>, 30Ni/*r*-CeO<sub>2</sub>, respectively. The numbers in front of the metals represent their respective loadings.

### 1.4 Measurements of catalytic activity

The hydrogenation reaction was carried out in a 50 mL stainless-steel high-pressure reactor. 250 mg of phenol, 0.1 g of catalyst and 25 mL of water were

charged into the autoclave. First, the reactor was purged with pure  $H_2$  three times to remove air. Then the reactor was charged with 3 MPa  $H_2$ , and the reaction was stirred at 150 °C for 16 h. After the reaction, the reactor was cooled to room temperature, and the remaining gas was carefully discharged. The reaction mixture was extracted with ethyl acetate and *n*-heptane as the internal standard. The content of the mixture was analyzed and the product was identified by GC-MS (Agilent Technologies 5975C and 7890A). The detecting condition was as follows: the injection port temperature was 280 °C; the detector temperature was 280 °C; the initial column temperature was 60 °C, and then heated to 250 °C at a heating rate of 20 °C/min.

### 1.5 Catalytic system recycling

300 mg of phenol, 200 mg of catalyst (15Ni-15Co/*r*-CeO<sub>2</sub>) and 25 mL of water were charged into the autoclave, then the reactor was charged with 3 MPa  $H_2$ , and the reaction was stirred at 150 °C for 16 h. After the reaction, the catalyst was washed three times with deionized water and dried overnight at 60 °C. Then the sample was reduced in  $H_2$  flow at 450 °C for 2 h. After that, the catalyst was used for the next run directly.

### 1.6 Catalyst characterization

Transmission electron microscopy (TEM) images were used to obtain the morphologies and sizes of all samples. X-ray powder diffraction (XRD) (X'pert, PANalytical, Dutch) was used to analyze the crystal-line structures of the samples, using Cu K $\alpha$  radiation ( $\lambda = 1.5406 \text{ \AA}$ ),  $2\theta$  ranges were 10°~90°. X-ray photoelectron spectroscopy (XPS) analyses were conducted on an X-ray photoelectron spectrometer (ESCALAB 250Xi) to detect the element compositions, the electron binding energy scale of all the spectra was calibrated using C 1s at 284.8 eV. Temperature programmed reduction (TPR) experiments were carried out with a TP-5080 characterization instrument with a TCD detector. Before the test, the samples (50 mg) were pretreated with an Ar flow (27 mL/min) at 300 °C for one hour and were then cooled down to 25 °C. The TPR test were performed by heating the samples in a  $H_2$ /Ar ( $H_2$ , 10%) mixture flow (30 mL/min). In

TPR, the temperature was increased from 25 to 900 °C with a linear heating ramp of 10 °C/min. The basicity and the basic strength distribution of the catalyst was studied by temperature programmed desorption of CO<sub>2</sub> (CO<sub>2</sub>-TPD) on a TP5080 apparatus. The samples were activated at 400 °C for 1 h prior to the adsorption of CO<sub>2</sub> at room temperature. After the physically adsorbed CO<sub>2</sub> was purged by a He flow at 120 °C, the samples were heated to 600 °C at the rate of 10 °C/min.

## 2 Result and Discussion

Fig.1 shows the typical transmission electron microscopy (TEM) image of the 30Co/*r*-CeO<sub>2</sub>, 30Ni/*r*-CeO<sub>2</sub> and 15Ni-15Co/*r*-CeO<sub>2</sub> catalysts. For 30Co/*r*-CeO<sub>2</sub> catalysts, it can be clearly seen that the lattice spacing of 0.21 and 0.286 nm are attributed to the (100) crystal plane of Co<sup>0</sup> and the (220) crystal plane of Co<sub>3</sub>O<sub>4</sub>, respectively, which indicated the presence of metallic Co<sup>0</sup> and Co<sub>3</sub>O<sub>4</sub>. It is likely that the presence of oxygen vacancies on CeO<sub>2</sub> prevents complete metal reduction. From Fig.1B, it can be noted that Ni<sup>0</sup> and NiO formed on the 30Ni/*r*-CeO<sub>2</sub> catalysts, and Ni<sup>0</sup> and NiO mainly exposes (111) and (200) crystal planes, respectively. As can be seen from Fig.1C, the lattice spacing of the catalyst was observed to be 0.209 and 0.268 nm, which were between 0.203~0.210 and 0.208~0.286 nm, suggesting that the presence of the alloying state in the 15Ni-15Co/*r*-CeO<sub>2</sub> sample<sup>[25]</sup>. The elemental mappings for Ni, Co, Ce, and O on the 15Ni-15Co/*r*-CeO<sub>2</sub> catalysts are shown in Fig.1D. It can be seen from the figure that the distribution of Ni and Co on *r*-CeO<sub>2</sub> is very similar, which further confirms the formation of the bimetallic composite.

Fig.2 shows the powder XRD patterns of the as-prepared NiCo/*r*-CeO<sub>2</sub> catalysts with different metal compositions. The feature peaks are observed at  $2\theta = 28.554^\circ, 33.081^\circ, 47.478^\circ, 56.334^\circ, 59.084^\circ, 69.400^\circ, 76.698^\circ, 79.067^\circ, 88.410^\circ$ , which correspond to the (111), (200), (220), (311), (222), (400), (331), (420), (422) plane diffraction patterns of the fluorite structure of CeO<sub>2</sub> (PDF #: 34-0394). Additionally, the XRD spectra could also prove the existence of Ni<sub>x</sub>Co<sub>y</sub>O and NiCo species. This

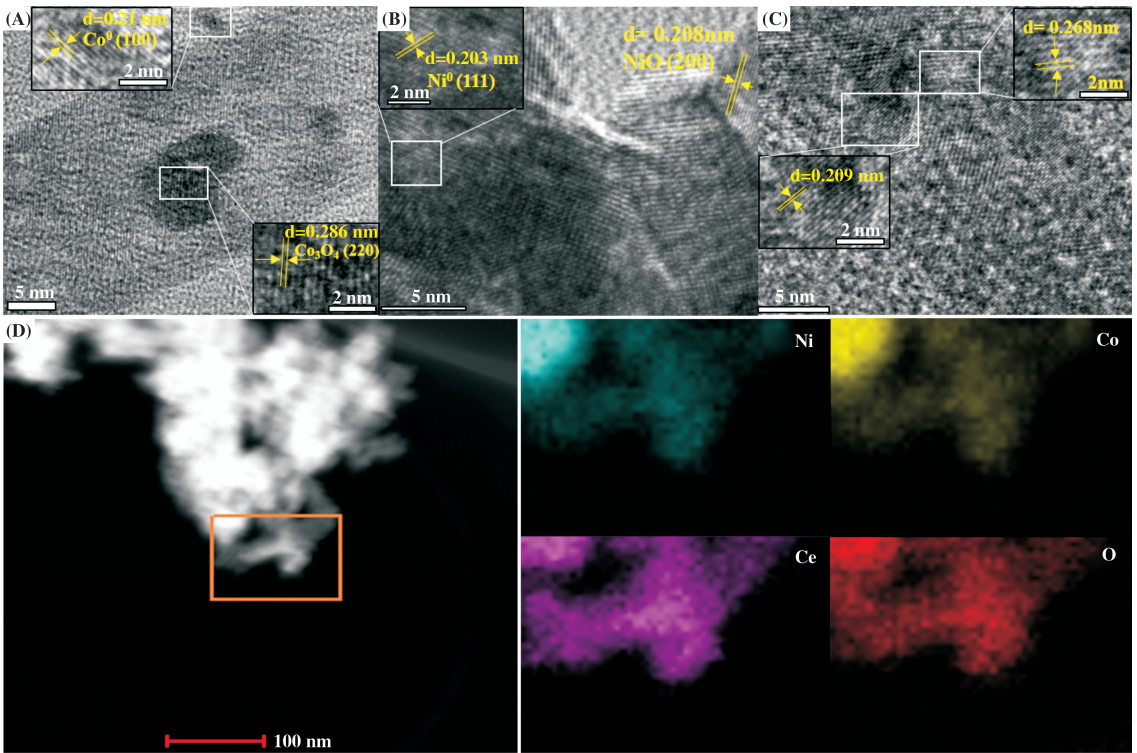


Fig.1 TEM images of (A) 30Co/*r*-CeO<sub>2</sub>, (B) 30Ni/*r*-CeO<sub>2</sub> and (C) 15Ni-15Co/*r*-CeO<sub>2</sub> catalysts, (D) Elemental mappings for Ni, Co, Ce, and O in 15Ni-15Co/*r*-CeO<sub>2</sub> catalysts

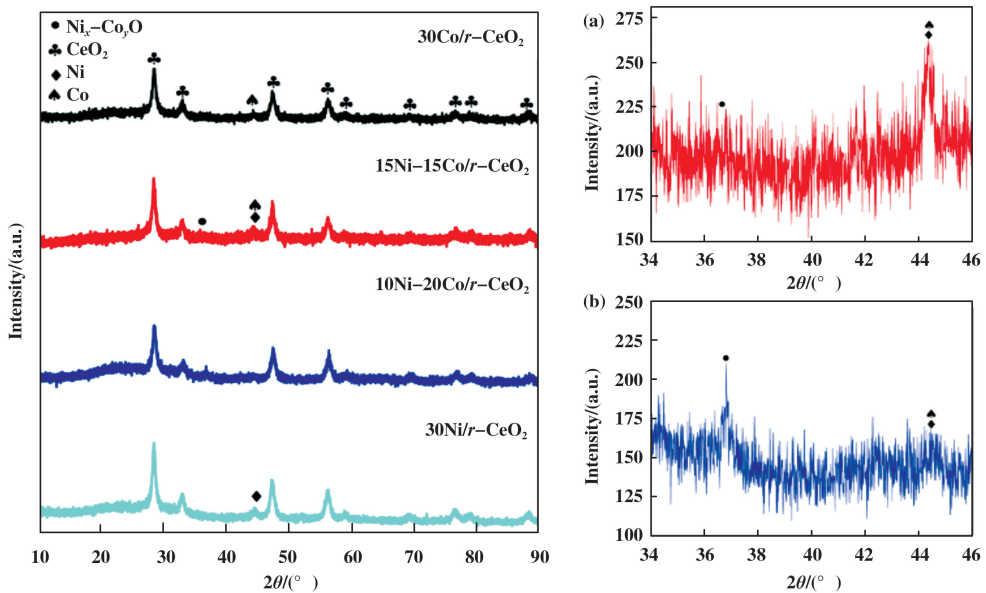


Fig.2 XRD patterns of the NiCo/*r*-CeO<sub>2</sub> catalysts with different metal compositions, (a) and (b) are partial enlarged views of 15Ni-15Co/*r*-CeO<sub>2</sub> and 10Ni-20Co/*r*-CeO<sub>2</sub>, respectively

may be the Co species in the bimetallic catalyst dissolves into the NiO lattice during the calcination to form the Ni<sub>x</sub>Co<sub>y</sub>O precursor, which partially forms the

Ni-Co alloy during the reduction process due to a large amount of oxygen vacancies on the *r*-CeO<sub>2</sub><sup>[26]</sup>. From Fig.2a and Fig.2b, as the amount of Co loading in-

creased, the intensity of the  $\text{Ni}_x\text{Co}_y\text{O}$  diffraction peak becomes stronger, which means that the relative content of  $\text{Ni}_x\text{Co}_y$  becomes higher. Meanwhile, the NiCo diffraction peaks became weaker, and it is possible that NiCo has better dispersibility or a smaller relative content. This is consistent with Shi's<sup>[20]</sup> report.

The  $\text{H}_2$ -TPR profile of the NiCo/*r*- $\text{CeO}_2$  catalysts with different metal compositions is shown in Fig.3.

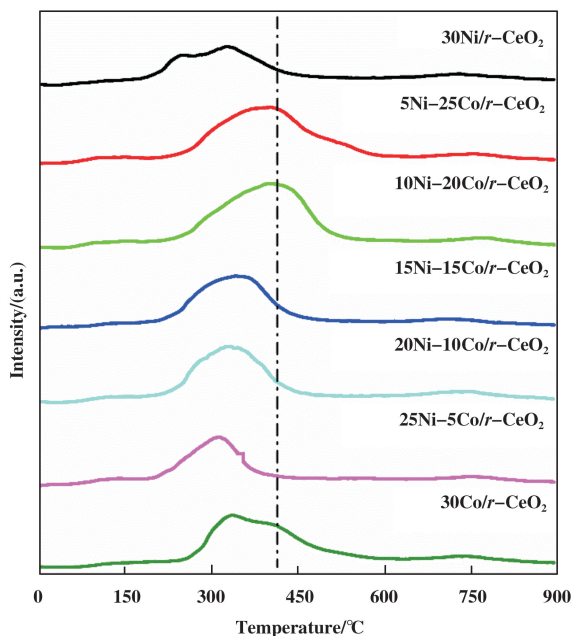


Fig.3  $\text{H}_2$ -TPR profile for the NiCo/*r*- $\text{CeO}_2$  catalysts with different metal compositions

The two reduction peaks at 336 and 412 °C for the monometallic Co/*r*- $\text{CeO}_2$  could be ascribed to the two step reduction process  $\text{Co}_3\text{O}_4 \rightarrow \text{CoO} \rightarrow \text{Co}^0$ . The monometallic Ni/*r*- $\text{CeO}_2$  profile showed two reduction peaks at 238 and 331 °C. The former could be associated with the reduction of bulk NiO clusters which weakly interacted with the exposed support surface, and the latter to the reduction of small NiO crystallites strongly bound to the  $\text{CeO}_2$  surface<sup>[27]</sup>. A broad peak between 600 and 800 °C in all the catalysts could be attributed to the reduction of the  $\text{CeO}_2$  support. For the bimetallic NiCo catalysts, the overlapped reduction peaks of cobalt oxide and nickel oxide were observed and the positions were shifted to different extents. It indicated that the electronic properties of the alloy surface are different from the electronic properties of the single metal sur-

face, resulting in different forces between the metal and the support.

We performed  $\text{CO}_2$ -TPD characterization of NiCo/*r*- $\text{CeO}_2$  catalysts. For monometallic Ni/*r*- $\text{CeO}_2$  and Co/*r*- $\text{CeO}_2$  catalysts, there are two broad  $\text{CO}_2$  desorption peaks at 100~200 and 350~550 °C, which attribute to weak and medium basic sites, respectively. In addition, the  $\text{CO}_2$ -TPD profiles of the NiCo bimetallic catalysts show one low-temperature desorption peak below 200 °C associated with the weak basicity which weakly absorbed  $\text{CO}_2$  on the catalyst surface. With the increase of Co content, the  $\text{CO}_2$  desorption peaks shift to low temperature, which implies that addition of cobalt reduces the catalysts surface basicity. In addition, we found that the number of basic sites on the 15Ni-15Co/*r*- $\text{CeO}_2$  catalyst was the smallest. Phenol is more easily co-planar adsorbed on the weakly basic site to form cyclohexanol<sup>[28]</sup>. This result could be ascribed to the fact that Co can give electrons to Ni, and the electron transfer effect between Co species and Ni species could improve the catalyst surface basicity. Therefore, the formation of the alloy facilitates the progress of the hydrogenation reaction and the formation of cyclohexanol.

The surfaces properties and chemical states of O, Ni and Co species on the catalysts surface were further measured by X-ray photoelectron spectroscopy (XPS). The 30Ni/*r*- $\text{CeO}_2$ , 15Ni-15Co/*r*- $\text{CeO}_2$  and 30Co/*r*- $\text{CeO}_2$  catalysts were characterized by XPS. Fig. 4a shows the high-resolution O 1s XPS spectra. The O 1s XPS data exhibit three peaks at 529.7 eV ( $\text{O}_L$ ), 531.4 eV ( $\text{O}_V$ ), and 532.6 eV ( $\text{O}_C$ ), which are assigned to the lattice oxygen bound to the metal cations,  $\text{O}^{2-}$  in oxygen-deficient regions, and chemisorbed or dissociated oxygen species or OH, respectively<sup>[29]</sup>. In general, the number of surface oxygen vacancies can be roughly estimated based on the ratio of  $\text{O}_V/\text{O}_L$ . The number of oxygen vacancies on the three catalysts is about 1.2, indicating that the oxygen vacancies have no effect on the catalytic activity of the catalyst. For both the 30Co/*r*- $\text{CeO}_2$  and 15Ni-15Co/*r*- $\text{CeO}_2$  catalysts (Fig.4b), the binding energy at around 791.6 and 779.6 eV could be indexed to the  $\text{Co}^0$ , and the peaks at around 797.3 and 781.6 eV could be ascribed to the Co  $2p_{1/2}$  and Co  $2p_{3/2}$

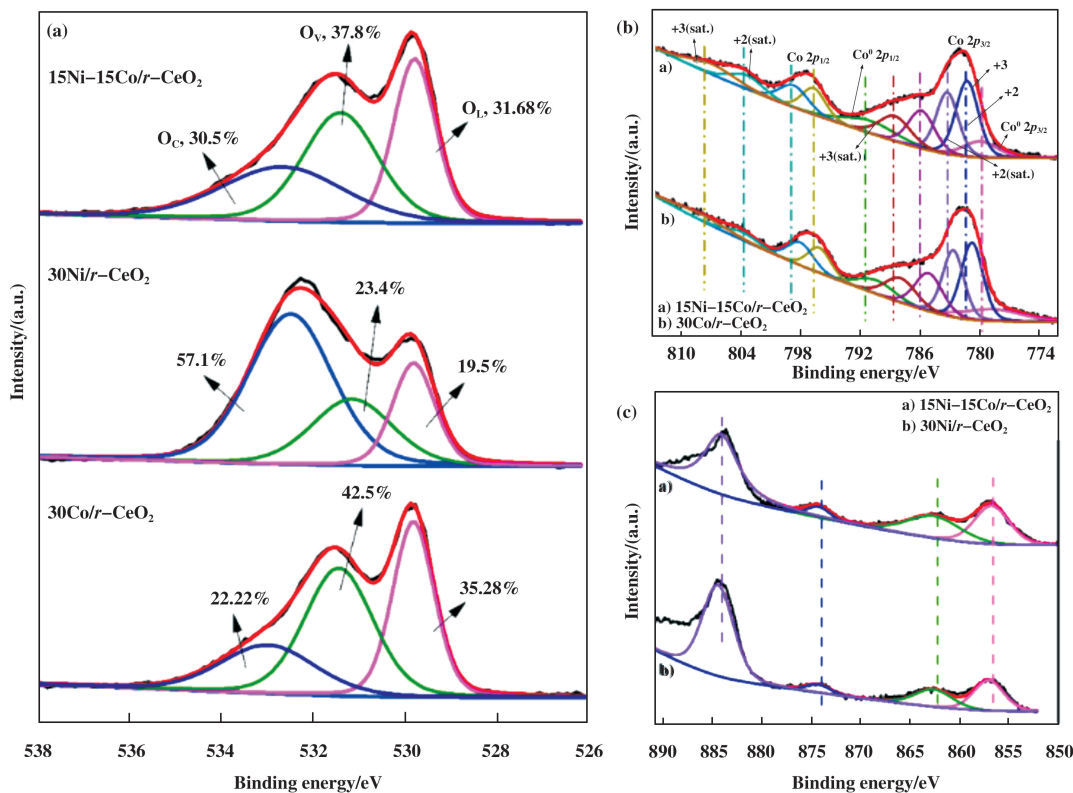


Fig.4 XPS spectra of O 1s (a), Co 2p (b) and Ni 2p (c) in 30Co/r-CeO<sub>2</sub>, 15Ni-15Co/r-CeO<sub>2</sub> and 30Ni/r-CeO<sub>2</sub> catalysts

of Co<sub>3</sub>O<sub>4</sub>, respectively. The peaks at around 804.8 and 787.5 eV could be ascribed to the satellite peaks<sup>[30]</sup>. In addition, a positive shift in binding energy was observed for the 15Ni-15Co/r-CeO<sub>2</sub> catalyst compared to the 30Co/r-CeO<sub>2</sub> catalyst, indicating that the alloying effect of the Co species and the Ni species causes a change in the electronic properties of Co. The Ni 2p XPS spectra of the 30Ni/r-CeO<sub>2</sub> and 15Ni-15Co/r-CeO<sub>2</sub> catalysts is shown in Fig.4c. As can be seen from the figure, the peaks with binding energies around 856.6 and 874.1 eV belong to Ni<sup>0</sup> 2p<sub>3/2</sub> and Ni<sup>0</sup> 2p<sub>1/2</sub>, respectively, and the peaks at around 862.6 and 884.1 eV correspond to Ni<sup>2+</sup> 2p<sub>3/2</sub> and Ni<sup>2+</sup> 2p<sub>1/2</sub>, respectively. There is also an overlap of satellite peaks around 884.1 eV. In detail, a negative shift in binding energy was also occurred for the 15Ni-15Co/r-CeO<sub>2</sub> catalyst compared to the 30Ni/r-CeO<sub>2</sub> catalyst, indicating that Ni gets a part of electrons into a rich electron state and causes the catalytic active center Ni to gener-

ate an unsaturated center. It's more conducive to the adsorption and desorption of hydrogen species<sup>[31]</sup>. At the same time, the results obtained by H<sub>2</sub>-TPR and CO<sub>2</sub>-TPD were confirmed. In a word, the formation of NiCo alloy changes the electronic states of Ni and Co, which may affect the catalytic performance of Ni and Co in the hydrogenation reaction. This will be confirmed by the evaluation results of the model reaction of phenol hydrogenation.

Hydrogenation of phenol as a model reaction for evaluation the catalytic performance of reduced mono- and bimetallic catalyst sample. Phenol conversion and product selectivity over different proportions of NiCo catalyst are shown in Fig.5. It is obvious that the selectivity of the cyclohexanol over all the catalysts is above 99.9% under the given reaction conditions (3.0 MPa H<sub>2</sub>, 150 °C). The selectivity of the NiCo bimetal catalyst supported on CeO<sub>2</sub> for cyclohexanol is better than that of NiCo/γ-Al<sub>2</sub>O<sub>3</sub><sup>[20]</sup> and NiCo/ZrO<sub>2</sub><sup>[32]</sup> catalysts.

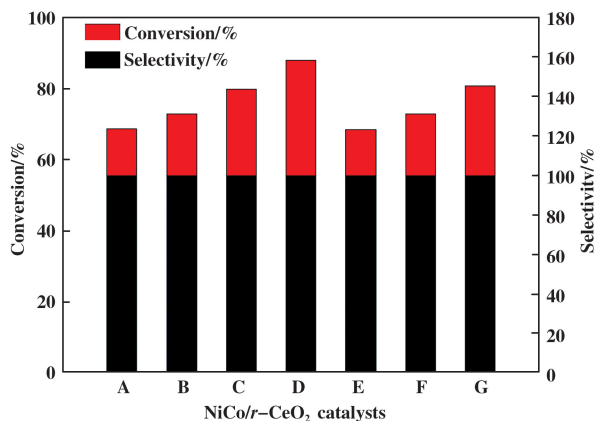


Fig.5 Phenol conversion and product selectivity over different catalysts

(A) 30Co/*r*-CeO<sub>2</sub>; (B) 5Ni-25Co/*r*-CeO<sub>2</sub>; (C) 10Ni-20Co/*r*-CeO<sub>2</sub>; (D) 15Ni-15Co/*r*-CeO<sub>2</sub>; (E) 20Ni-10Co/*r*-CeO<sub>2</sub>; (F) 25Ni-5Co/*r*-CeO<sub>2</sub>; (G) 30Ni/*r*-CeO<sub>2</sub>

Compared with the 30Co/*r*-CeO<sub>2</sub> catalyst, the catalytic activity increased significantly with the increase of nickel content. For the 30Ni/*r*-CeO<sub>2</sub> catalyst, the catalytic activity decreases as the cobalt content increases, and the activity of the single metal Co catalyst is the lowest (68.6%) among all the as-prepared catalysts. This indicates that Ni species is more active than Co species for hydrogenation of phenol reaction. However, when the loading of nickel and cobalt is the same (15%), the conversion of phenol is higher (88%) than other catalysts, which means the mass fraction of Ni and Co has a great influence on the catalytic activity. There are two mechanisms for phenol activation, “two-site”<sup>[33]</sup> adsorption and “one site”<sup>[34]</sup> adsorption. From H<sub>2</sub>-TPR result, we can know that 15Ni-15Co/*r*-CeO<sub>2</sub> catalyst has better activity for phenol hydrogenation, but its ability to activate hydrogen is not significantly different from other catalysts. This indicates that the activation of phenol on NiCo bimetal catalysts is mainly “one site” adsorption, that is, both phenol and hydrogen are adsorbed on the metal site. Hence, the high activity of 15Ni-15Co/*r*-CeO<sub>2</sub> in catalyzing phenol hydrogenation is most likely due to the strong activation ability of phenol. Combining characterization results, it is more likely that the addition of cobalt modulates the surface properties for the active site of the catalyst, so

that the catalytic activity of the NiCo bimetallic catalyst at an appropriate ratio (Ni : Co = 1 : 1) is higher than that of the single metal catalyst.

To further investigate the difference in activity between bimetallic and single metal catalysts, 30Ni/*r*-CeO<sub>2</sub>, 30Co/*r*-CeO<sub>2</sub> and 15Ni-15Co/*r*-CeO<sub>2</sub> catalysts were chosen to study the kinetic behavior of phenol hydrogenation to cyclohexanol. The apparent activation energy on 15Ni-15Co/*r*-CeO<sub>2</sub> is 15.04 kJ/mol, which is smaller than that on 30Ni/*r*-CeO<sub>2</sub> (23.2 kJ/mol) and 30Co/*r*-CeO<sub>2</sub> (96.1 kJ/mol) catalysts. The smaller the activation energy, the lower the activation barrier that is required to pass from the reactant to the product, indicating that the hydrogenation of phenol reaction is greatly improved over the 15Ni-15Co/*r*-CeO<sub>2</sub> catalyst. Otherwise, the stability of the catalytic system for 15Ni-15Co/*r*-CeO<sub>2</sub> catalyst was also investigated by the hydrogenation of phenol. After recycling five times, the activity of the catalytic system was not significantly reduced, and the phenol conversion were all around 60%, which confirmed that 15Ni-15Co/*r*-CeO<sub>2</sub> catalyst is stable under the reaction conditions. Hence, the Co-doped NiCo/*r*-CeO<sub>2</sub> catalyst is likely to be a good candidate for the hydrogenation of phenol to cyclohexanol.

### 3 Conclusion

In summary, a series of NiCo bimetallic catalysts with different mass ratios supported on nanorod CeO<sub>2</sub> were prepared by a simple wet chemical impregnation method. It was found that the activity of NiCo bimetallic catalyst at a suitable mass ratio (Ni : Co = 1 : 1) for the hydrogenation reaction of phenol is higher than that of the corresponding single metal catalysts, which can attribute to the addition of cobalt increases the dispersion of Ni species and modulates the surface properties of active sites on the catalysts. Co-doped NiCo catalysts are expected to provide guidance in the design of high activity phenol hydrogenation catalysts.

#### Acknowledgements:

This research was financially supported by the CAS “Light of West China” Program.

#### References:

[1] Yan N, Yuan Y, Dykeman R, *et al.* Hydrode oxygenation

- of lignin-derived phenols into alkanes by using nanoparticle catalysts combined with bronsted acidic ionic liquids [J]. *Angew Chemie-Inter Ed*, 2010, **49** (32): 5549–5553.
- [2] Zhao C, He J, Lemonidou A A, *et al.* Aqueous-phase hydrodeoxygenation of bio-derived phenols to cycloalkanes [J]. *J Catal*, 2011, **280**(1): 8–16.
- [3] Luska K L, Migowski P, El Sayed S, *et al.* Synergistic interaction with in bifunctional ruthenium nanoparticle/SILP catalysts for the selective hydrodeoxygenation of phenols[J]. *Angew Chemie-Inter Ed*, 2015, **54** (52): 15750–15755.
- [4] He J, Lu X H, Shen Y, *et al.* Highly selective hydrogenation of phenol to cyclohexanol over nano silica supported Ni catalysts in aqueous medium [J]. *Mol Catal*, 2017, **440**: 87–95.
- [5] Besson M, Gallezot P, Pinel C. Conversion of biomass into chemicals over metal catalysts [J]. *Chem Reviews*, 2014, **114**(3): 1827–1870.
- [6] Kang L, Guo J, Zhang H, *et al.* Activity and stability of Ni/SiO<sub>2</sub>-Al<sub>2</sub>O<sub>3</sub> catalyst in the aqueous phase hydrogenation system ST [J]. *J Mol Catal(China)*, 2014, **28**(2): 119–125.
- [7] Zhao F, Wang C, Tian Y, *et al.* Metal promoter effect of Ni-M/SiO<sub>2</sub> in hydrogenation of 1,4-butanediol [J]. *J Mol Catal(China)*, 2019, **33**(1): 83–89.
- [8] Wang Y, Luo G, Xu X, *et al.* Preparation of supported skeletal Ni catalyst and its catalytic performance on dicyclopentadiene hydrogenation [J]. *Catal Commun*, 2014, **53**: 15–20.
- [9] Yuan X, Song H. Progresses in synthesis and application of Ni-based bimetallic catalysts [J]. *Petrochem Technol*, 2017, **46**(8): 1089–1096.
- [10] Alonso D M, Wettstein S G, Dumesic J A. Bimetallic catalysts for upgrading of biomass to fuels and chemicals [J]. *Chem Soc Rev*, 2012, **41**(24): 8075–8098.
- [11] Li X, Wan W, Chen J G, *et al.* Selective hydrogenation of biomass-derived 2(5H)-furanone to gamma-butyrolactone over Ni-based bimetallic catalysts [J]. *Acs Sust Chem & Eng*, 2018, **6**(12): 16039–16046.
- [12] Jia P, Lan X, Li X, *et al.* Highly active and selective NiFe/SiO<sub>2</sub> bimetallic catalyst with optimized solvent effect for the liquid-phase hydrogenation of furfural to furfuryl alcohol [J]. *Acs Sust Chem & Eng*, 2018, **6**(10): 13287–13295.
- [13] Ray K, Deo G. A potential descriptor for the CO<sub>2</sub> hydrogenation to CH<sub>4</sub> over Al<sub>2</sub>O<sub>3</sub> supported Ni and Ni-based alloy catalysts [J]. *Appl Catal B-Environ*, 2017, **218**: 525–537.
- [14] Tian Y, Zhao F, Wang C, *et al.* Effect of Cu additive on the hydrogenation of 1, 4-butanediol over Ni-Cu/SiO<sub>2</sub> bimetallic catalyst [J]. *J Mol Catal(China)*, 2019, **33** (2): 132–139.
- [15] Zhao X, Walker D M, Maiti D, *et al.* NiMg/ceria-zirconia cylindrical pellet catalysts for tri-reforming of surrogate biogas [J]. *Indus & Eng Chem Res*, 2018, **57**(3): 845–855.
- [16] Ibrahim A M M, Shi X, Radwan A R, *et al.* Enhancing the tribological properties of NiAl based nano-composites for aerospace bearing applications [J]. *Mater Res Express*, 2019, **6**(8): 085067.
- [17] Gonzalez-Delacruz V M, Pereniguez R, Ternero F, *et al.* In situ XAS study of synergic effects on Ni-Co/ZrO<sub>2</sub> methane reforming catalysts [J]. *J Phys Chem C*, 2012, **116**(116): 2919–2926.
- [18] Shimura K, Miyazawa T, Hanaoka T, *et al.* Fischer-tropsch synthesis over alumina supported bimetallic Co-Ni catalyst; Effect of impregnation sequence and solution [J]. *J Mol Catal A Chem*, 2015, **407**: 15–24.
- [19] Xie Y, Xiao N, Ling Z, *et al.* Flower-like Co-Ni/C bimetallic catalysts for the selective hydrogenation of o-chloronitrobenzene [J]. *Chin J Catal*, 2012, **33**(12): 1883–1888.
- [20] Shi Y, Chen S, He L, *et al.* Selective conversion of phenol in a subcritical water medium using gamma-Al<sub>2</sub>O<sub>3</sub> supported Ni-Co bimetallic catalyst [J]. *Catal*, 2019, **9** (3): 212.
- [21] Ha H, Yoon S, An K, *et al.* Catalytic CO oxidation over Au nanoparticles supported on CeO<sub>2</sub> nanocrystals: Effect of the Au-CeO<sub>2</sub> interface [J]. *Acs Catal*, 2018, **8**(12): 11491–11501.
- [22] Pei Xiao-ping (裴晓平), Ma Zhan-wei (马占伟), Song Chen-li (宋承立), *et al.* Effect of interface regulation between Ru and the Ce<sub>0.8</sub>Pr<sub>0.2</sub>O<sub>2</sub> support on the activity of ammonia synthesis [J]. *J Mol Catal(China)*, 2018, **32** (3): 195–204.
- [23] Lv Y, Li N, Ma Q, *et al.* Effect of preparation methods on the performance of the Co<sub>3</sub>O<sub>4</sub>-CeO<sub>2</sub> catalyst [J]. *J Mol Catal(China)*, 2010, **24**(5): 450–455.
- [24] Ma Z, Zhao S, Pei X, *et al.* New insights into the support morphology-dependent ammonia synthesis activity of Ru/CeO<sub>2</sub> catalysts [J]. *Catal Sci & Technol*, 2017, **7** (1): 191–199.
- [25] Zhang Z, Yang Q, Chen H, *et al.* In situ hydrogenation

- and decarboxylation of oleic acid into heptadecane over a Cu-Ni alloy catalyst using methanol as a hydrogen carrier [J]. *Green Chem*, 2018, **20**(1): 197–205.
- [26] Wu H, Liu H, Yang W, *et al.* Synergetic effect of Ni and Co in Ni-Co/SBA-15-CD catalysts and their catalytic performance in carbon dioxide reforming of methane to syngas[J]. *Catal Sci & Technol*, 2016, **6**(14): 5631–5646.
- [27] Xiang J, Wen X, Zhang F. Supported nickel-cobalt bimetallic catalysts derived from layered double hydroxide precursors for selective hydrogenation of pyrolysis gasoline[J]. *Indus & Eng Chem Res*, 2014, **53**(40): 15600–15610.
- [28] Velu S, Kapoor M P, Inagaki S, *et al.* Vapor phase hydrogenation of phenol over palladium supported on mesoporous CeO<sub>2</sub> and ZrO<sub>2</sub>[J]. *Appl Catal A-Gen*, 2003, **245**(2): 317–331.
- [29] Liu D, Li G, Yang F, *et al.* Competition and cooperation of hydrogenation and deoxygenation reactions during hydrodeoxygenation of phenol on Pt(111)[J]. *J Phys Chem C*, 2017, **121**(22): 12249–12260.
- [30] Dong G, Hu H, Huang X, *et al.* Rapid activation of Co<sub>3</sub>O<sub>4</sub> cocatalysts with oxygen vacancies on TiO<sub>2</sub> photocatalysts for efficient water splitting[J]. *J Mater Chem A*, 2018, **6**(42): 21003–21009.
- [31] Zhang Yu-qiao (张玉娇), Yao Jian-long (姚建龙), Hu Feng-teng(胡凤腾), *et al.* Catalytic performance of supported NiFe bimetallic catalyst for selective hydrogenation of phenol[J]. *Mod Chem Indus*, 2018, **38**(11): 178–182.
- [32] He L, Niu Z, Miao R, *et al.* Selective hydrogenation of phenol by the porous Carbon/ZrO<sub>2</sub> supported Ni-Co nanoparticles in subcritical water medium[J]. *J Cleaner Product*, 2019, **215**: 375–381.
- [33] Neri G, Visco A M, Donato A, *et al.* Hydrogenation of phenol to cyclohexanone over palladium and alkali-doped palladium catalysts [J]. *Appl Catal A-Gen*, 1994, **110**(1): 49–59.
- [34] Chen Y Z, Liaw C W, Lee L I. Selective hydrogenation of phenol to cyclohexanone over palladium supported on calcined Mg/Al hydrotalcite [J]. *Appl Catal A-Gen*, 1999, **177**(1): 1–8.

## CeO<sub>2</sub> 负载 NiCo 双金属催化苯酚液相加氢

鲁金芝<sup>1,2</sup>, 马占伟<sup>1</sup>, 魏雪梅<sup>1,2</sup>, 张勤生<sup>1</sup>, 胡斌<sup>1\*</sup>

(1. 中国科学院兰州化学物理研究所 羰基合成与选择氧化国家重点实验室, 甘肃 兰州 730000;

2. 中国科学院大学, 北京 100049)

**摘要:** 采用湿化学浸渍法制备了 CeO<sub>2</sub> 纳米棒负载的 CoNi 双金属催化剂, 并研究了其在 150 °C, 3 MPa H<sub>2</sub> 下对苯酚加氢成环己醇反应的催化活性, 发现具有合适 NiCo 质量比的 NiCo/*r*-CeO<sub>2</sub> 催化剂显示出比单金属催化剂高的催化活性. 通过 TEM 和 XRD 证明了 NiCo 合金的形成和高分散性, H<sub>2</sub>-TPR 和 CO<sub>2</sub>-TPD 揭示了合金中钴和镍之间的电子相互作用导致金属与载体之间的相互作用力发生变化, XPS 也表明 NiCo 合金中 Ni 和 Co 的电子态也发生了变化. 结合表征结果和双金属催化剂催化苯酚加氢反应的活性, 表明添加 Co 可以调节活性部位的表面性能, 进而影响 NiCo 双金属催化剂在苯酚加氢反应中的催化活性.

**关键词:** 钴; 镍; 双金属; 苯酚加氢; 电子效应